


Enhancement of thermionic power generation via engineered microstructures

Chace Franey¹, Bakir M. Al-Ameri¹, Greg I. Acosta¹, and Mohammad Ghashami^{1*}

Department of Mechanical and Materials Engineering, University of Nebraska-Lincoln, Lincoln, Nebraska 68588, USA

 (Received 20 July 2023; revised 20 November 2023; accepted 17 January 2024; published 1 February 2024)

Thermionic energy conversion has attracted significant attention in recent years thanks to improvements enabled by microfabrication techniques and advanced materials. As society moves towards a more-environment-friendly future, thermionic energy converters (TECs) could be a competitive option for clean energy generation by recycling wasted heat from various thermal systems. Reducing the interelectrode gap to a few micrometers has recently been proposed to improve the performance of TECs by mitigating the effect of negative space charge. Moreover, adding microscale features onto the surface of a TEC's emitter is another way to improve the device's performance significantly. The presence of microstructures on the emitter can increase the effective emitting surface area and enhance the effects of Schottky barrier lowering. Despite their advantages, no theoretical framework exists presenting an in-depth analysis of the effect of microscale features on a TEC. This study presents a theoretical framework considering microscale hyperboloidal emitter surface features for a TEC with a microscale interelectrode gap. Considering their impact on the maximum potential barrier, emitting surface area, and near-field radiative heat transfer, we show that the maximum output power density can be increased by a factor of approximately 2 when the plane-to-plane gap distance and the periodicity are both $0.5\ \mu\text{m}$ compared with a TEC with a planar emitter. Despite the significant increase in output power density, the increase in efficiency is minimal due to the increase in the thermal radiative heat flux. The present work provides a theoretical framework for analyzing TECs equipped with surface-engineered emitters that can significantly increase and control the output power density, pushing thermionic energy conversion towards becoming a more-practical means of energy conversion.

DOI: [10.1103/PhysRevApplied.21.024004](https://doi.org/10.1103/PhysRevApplied.21.024004)

I. INTRODUCTION

Thermionic energy converters (TECs) generate electricity by collecting electrons that are thermally emitted over the potential-energy barrier of a high-temperature cathode, referred to as the emitter. Until the 1990s, thermionic energy conversion was extensively researched for its use in space missions [1,2]. Although much progress was made, the limited power throughput and low efficiency (less than 15%) of TECs caused interest in the technology to decline towards the end of the century [2]. The need for low-work-function electrode materials that can withstand high temperatures (more than 1000 K) was a major bottleneck in the earlier designs of TECs. Additionally, the buildup of negative space charge (NSC) in the interelectrode gap caused by the traversing electrons hindered high electron emission rates [1,3–5]. As a result, several methods have been proposed to mitigate the effect of NSC, including pumping ignited cesium plasma into the interelectrode gap [1,6], using an electron-accelerating gate or grid [1,7,8],

or replacing the vacuum with a thin semiconductor material (less than $1\ \mu\text{m}$) [9]. Despite their potential, these methods are challenging to implement and have a limited effect on the achievable efficiency [1,10]. Recent studies have demonstrated that reducing the interelectrode gap to a few micrometers can mitigate the effect of NSC without requiring additional components [4,11–14]. At such small gaps, new physical phenomena emerge that must be carefully considered when one is evaluating the performance of TECs. For instance, (near-field) radiative heat transfer between the electrodes can surpass the classical blackbody limit when the separation distance is smaller than the thermal characteristic wavelength [15,16]. Other phenomena, such as the image-charge effect and electron tunneling, can also play a role if the gap is even smaller and within nanometers [4,5,11].

Numerous theoretical studies have investigated the gap-dependent charge and thermal radiative transport mechanisms in TECs. Apart from demonstrating promising performance improvements, these studies revealed the trade-off between the adverse effects of near-field thermal radiation and increased electron emission rates as the gap distance reduces to a few micrometers

*mghashami2@unl.edu

[4,5,12–14,17]. A handful of experimental studies have investigated microgap TECs by using microfabricated spacers and demonstrated their feasibility as a means to create a device-level TEC [18–22]. However, the large parasitic heat conduction through the spacers resulted in limited efficiencies compared with the theoretical predictions. Other experiments have used micropositioning stages to control the interelectrode gap distance [23–25]; however, achieving single-micrometer gaps while maintaining a significant temperature gradient proved challenging.

While previous studies focused on TECs with planar electrode surfaces, there is little discussion about the possible advantages of modifying the surface topography of the electrodes. Apart from studies where electron reflection is considered [4,12,26,27], TECs with surface-engineered electrodes have not been extensively explored despite their great potential. Notably, the addition of certain microscale features on the emitter surface can augment the effects of Schottky barrier lowering, facilitating electron emission due to higher electric fields and electrostatic interactions [4,5,11]. The effects of implementing electric-field-enhancing surface features have been studied in detail for their applications towards field emitters [11,28–33], but there exist very limited studies on their application in thermionic emission and energy conversion [34–37]. Because of the difficulty in analytically calculating a nonplanar electrode's local electric field strength, the studies investigating their applications towards thermionic emission have been done computationally [34,35] or experimentally [36,37]. These studies have conclusively shown how engineering the emitter surface can enhance electron emission, although their lack of analytical solutions limits their applicability to a wide range of surface feature geometries.

In this article, we present a theoretical framework evaluating the performance of TECs with engineered emitter surfaces. We consider uniform hyperboloidal protrusions

on the emitter surface where an exact solution for the electric field along their surface can be found using the prolate-spheroidal coordinate system [32,33]. The effect of introducing these tips on electron emission is found by considering the enhancement of the electric field and the increase in the effective surface area. Additionally, their effect on near-field thermal radiation is determined by evaluating the effective optical properties of the engineered emitter surface. For our analysis throughout this work, we consider the work function of the emitter ϕ_E and the temperature of the emitter T_E to be 2.1 eV and 1500 K, respectively, and the work function of the collector ϕ_C and the temperature of the collector T_C to be 1.2 eV and 750 K, respectively. These values agree with the correlation $600 < T/\phi < 800$ described by Hatsopoulos and Gyftopoulos [1], and are within the practical range for a TEC [10]. The work functions and temperatures chosen enable us to compare our results with the results of other theoretical studies using similar parameters [4,5,12,13,17]. The knowledge gained from this study allows us to design engineered surfaces that could significantly increase the power throughput of TECs.

II. THEORETICAL FRAMEWORK

A. General overview of thermionic energy conversion

Figure 1(a) shows a simple schematic of a TEC with microscale emitter surface features. The net current density, J , of a TEC where back emission is present is governed by [1]

$$J = J_{EC} - J_{CE} = A_{\text{RLD}} \left[T_E^2 \exp\left(\frac{-\psi_m}{k_B T_E}\right) - T_C^2 \exp\left(\frac{-(\psi_m - eV)}{k_B T_C}\right) \right], \quad (1)$$

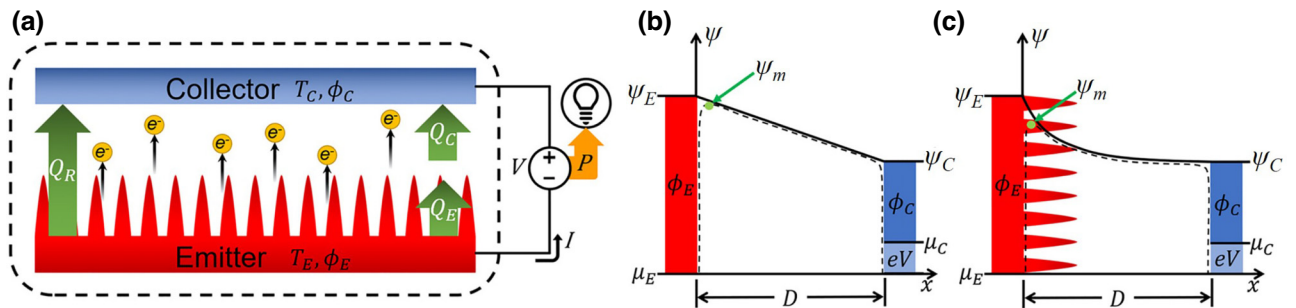


FIG. 1. (a) TEC consisting of an emitter with surface features and a flat collector. The temperatures and the work functions of the emitter and collector are fixed. The energies exchanged between the electrodes consist of the thermal radiative heat transfer and the energy carried by the electrons—part of which is converted to electric power. (b),(c) Energy diagrams showing the expected potential profile (b) before the addition of hyperboloidal tips and (c) after the addition of hyperboloidal tips, where μ_i is the electrodes' Fermi levels, ψ_i is the electrodes' potentials, and ψ_m is the maximum potential. Subscript $i = E$ stands for the emitter and subscript $i = C$ stands for the collector.

where J_{EC} (J_{CE}) is the current density from the emitter (collector) to the collector (emitter), $A_{RLD} = 120 \text{ A cm}^{-2} \text{ K}^{-2}$ is the Richardson-Laue-Dushman constant, k_B is the Boltzmann constant, T_E and T_C are the surface temperatures of the emitter and collector, respectively, V is the applied voltage between electrodes, e is the unit charge, and ψ_m is the maximum potential barrier electrons need to overcome. The maximum potential is largely determined by the electrode material's work function, ϕ , but other factors, such as the interelectrode gap distance, D , and the applied voltage, V , can alter the potential profile as well. The resultant potential profile within the interelectrode gap, $\psi(x)$, can be found by solving the one-dimensional Poisson equation [1,3–5,11],

$$\frac{d^2\psi(x)}{dx^2} = -\frac{e^2 n(x)}{\epsilon_0}, \quad (2)$$

where x is the position between the emitter ($x = 0$) and the collector ($x = D$), $n(x)$ is the electron density as a function of x , and ϵ_0 is the vacuum permittivity.

On the basis of previous studies, the effect of NSC becomes negligible at small gap distances ($D < 2 \text{ }\mu\text{m}$) [4,5,12–14,17]. In this range of gap distances, the potential can be approximated as a straight-line potential profile, as shown in Fig. 1(b) [1,4,5]. At such small gap distances, the image-charge effect can become more prominent, and the resulting potential profile is then found from [11]

$$\psi(x) = \psi_{m,0} - Fx - \frac{Q}{x}, \quad (3)$$

where $\psi_{m,0}$ is the maximum potential before the inclusion of image charge, F is the local electric field strength, and $Q = e^2/16\pi\epsilon_0$ is a constant. The terms $-Fx$ and $-Q/x$ in Eq. (3) convey the roles that the electric field and the image-charge Coulomb potential, respectively, play in the image-charge effect [11]. In the absence of NSC, $\psi_{m,0} = \phi_E$ if $V \leq \phi_E - \phi_C$, otherwise $\psi_{m,0} = \phi_C + eV$. Solving for the value of x at which $\partial\psi(x)/\partial x = 0$ yields the maximum potential [11],

$$\psi_m = \psi_{m,0} - \sqrt{4QF}, \quad (4)$$

where $\sqrt{4QF}$ is defined as the Schottky-barrier-lowering factor. Equation (4) shows that a higher electric field results in a lower maximum potential and, ergo, results in a higher current density. Hence, a clear benefit is gained from adding surface features that enhance the electric field, as shown in Fig. 1(c). In this study, our analysis specifically targets gap distances of $D \leq 1\text{ }\mu\text{m}$. This focus is driven by the fact that such narrow gaps more effectively illustrate the critical influence of the tips on power outputs in TEC applications and are particularly relevant in the context of microstructured surfaces. We deem the NSC effect negligible within this range, streamlining our initial analysis.

Given the complexities involved in accurately incorporating the NSC effect for microstructured surfaces, especially in the absence of a definitive analytical method, our study does not attempt to address this challenge directly. Instead, in the final section, we offer a simplified discussion on NSC, demonstrating that its impact on power output is likely to be negligible for such small gap distances.

B. Local electric field and potential barrier on a hyperboloidal tip's surface

To investigate the effect of microstructures on the performance of TECs, we consider periodic arrays of hyperboloidal tips on the emitter surface. Our analysis of the electric field strength along the surface of a hyperboloidal tip is built upon a solution derived in prolate-spheroidal coordinates [32,33]. The solution for the electric field strength is dependent on the tip's half-angle, θ , the tip apex's radius of curvature, r , and the position along the surface of the tip, s , which are illustrated in the inset in Fig. 2(a). Here, s is an orthogonal coordinate of the prolate-spheroidal coordinate system, where $s = 1$ at the apex of the tip and $s = s_0$ at the junction where the tip and planar surface of the emitter meet. For a tip of height h and base radius R on a TEC with plane-to-plane gap distance D , s_0 , θ , and r can be found using the following expressions [33,38]:

$$s_0 = \frac{D}{D-h} = \frac{D}{d}, \quad (5a)$$

$$\theta = \tan^{-1}\left(\frac{R}{\sqrt{D^2 - d^2}}\right), \quad (5b)$$

$$r = d \tan^2 \theta, \quad (5c)$$

using these relationships, the electric field as a function of s is then found to be given by [33]

$$F(s) = \frac{V_0}{r} \frac{\tan \theta}{Q_{\cos \theta} \sqrt{s^2 - \cos^2 \theta}}, \quad (6)$$

where $V_0 = (\phi_E - \phi_C)/e - V$ is the internal voltage drop [1] and $Q_{\cos \theta} = \frac{1}{2} \ln [(1 + \cos \theta)/(1 - \cos \theta)]$. Equation (6) is valid only when the electric field is positive ($V_0 > 0$). To find the average electric field across the tip, the physical dimensions of the feature must be accounted for by integration across s and the azimuthal angle of rotation about the axis of symmetry of the tip, α , and dividing it by the tip's surface area, S_{tip} . This is done with the use of geometric scale factors $h_s(s)$ and $h_\alpha(s)$, given by [38]

$$h_s(s) = a \sqrt{\frac{s^2 - \cos^2 \theta}{s^2 - 1}}, \quad (7a)$$

$$h_\alpha(s) = d \tan \theta \sqrt{s^2 - 1}, \quad (7b)$$

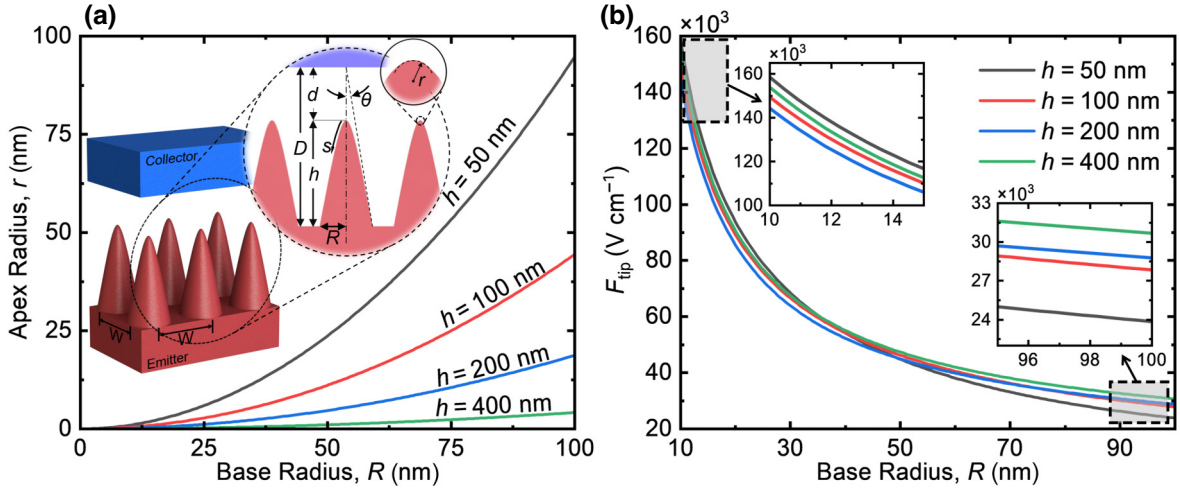


FIG. 2. (a) Dependence of the apex radius (r) on the base radius (R) for various tip heights (h). The inset shows a schematic of the geometrical parameters of the hyperboloidal tips in a square packing scheme with periodicity length W . (b) Average tip electric field as a function of the base radius for four different tip heights for an applied voltage V of 0.5 V and a gap distance D of 0.5 μm .

where $a = d / \cos \theta$ is the half-focus distance of the hyperboloid. The average electric field across the tip is then found using the following expression:

$$F_{\text{tip}} = \frac{2\pi \int_1^{s_0} F(s) h_s(s) h_\alpha(s) ds}{S_{\text{tip}}} = \frac{\int_1^{s_0} F(s) h_s(s) h_\alpha(s) ds}{\int_1^{s_0} h_s(s) h_\alpha(s) ds}. \quad (8)$$

As shown in Fig. 2(b), the value of h that results in the highest F_{tip} value reduces as R gets smaller. Although $F(s)$ displays an inverse relationship with r [Eq. (6)], the value of h that results in the smallest value of r [see Fig. 2(a)] does not necessarily result in the largest value of F_{tip} . This can be explained by our noting that as R gets smaller, the inverse relationship of F_{tip} with S_{tip} becomes dominant over the inverse relationship of $F(s)$ with r . Regardless of the tip geometries presented in Fig. 2(b), F_{tip} is at least twice that of an emitter with no surface features ($F_{\text{flat}} = V_0/D$). The maximum potential along the tip surface, $\psi_m(s)$, can be found by substituting Eq. (6) into Eq. (4). The behavior of $\psi_m(s)$ along the surface of the emitter is shown in Fig. 3(a) for the value of R that results in the smallest average maximum potential, $\psi_{m,\text{av}}$, for a given D , W , and h . Figure 3(a) shows that the smallest value of $\psi_{m,\text{av}}$ is not achieved with a value of R where $F(s)$ is largest, i.e., where r is smallest. Furthermore, the amount by which ψ_m is decreased is less than 0.15 eV at any point along the surface.

C. Enhanced thermionic emission

Knowing $\psi_m(s)$, we can find the thermionically emitted current density along the tip surface, $J(s)$, from Eq. (1). Integrating $J(s)$ over s and α , we find the total current

across the entire tip is given by

$$I_{\text{tip}} = 2\pi \int_1^{s_0} J(s) h_s(s) h_\alpha(s) ds. \quad (9)$$

To calculate the effective current density, the total current emitted from the tip is plane-averaged by dividing it by the base area, $J_{\text{tip}} = I_{\text{tip}}/\pi R^2$. In this study, we choose a square packing scheme for simplicity, where the flat area surrounding the tip is determined by $W^2 - \pi R^2$, where W represents the side length of the square [see Fig. 2(a)]. On the flat area without the tips, the only Schottky barrier lowering that occurs is due to the nonenhanced electric field, F_{flat} . Thus, the current density emitted from the flat area, J_{flat} , is calculated by inserting the corresponding maximum potential, $\psi_{m,\text{flat}}$, into Eq. (1). $\psi_{m,\text{flat}}$ is obtained by substituting F_{flat} into Eq. (4). The plane-averaged current density over the entirety of the square area can then be determined from the following expression:

$$J_{\text{tot}} = \frac{1}{W^2} [\pi R^2 J_{\text{tip}} + (W^2 - \pi R^2) J_{\text{flat}}]. \quad (10)$$

Figure 3(b) demonstrates that J_{tot} increases as R and h get larger. The output power density, found from $P = J_{\text{tot}} V$, shows similar behavior, as seen in Fig. 3(c). If Schottky barrier lowering were the primary source of enhancement, then it would be expected that the greatest output performance would be seen at smaller base radii due to the inverse relationship of $F(s)$ with r . Contrary to this, it is observed that the maximum current and power densities occur at the largest tip surface areas.

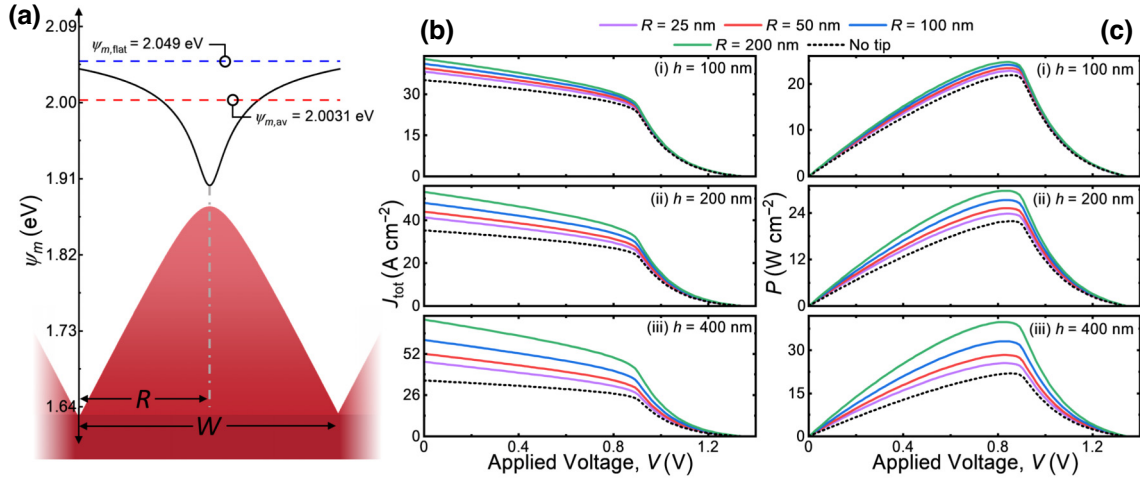


FIG. 3. (a) Maximum potential (ψ_m) at an applied voltage V of 0 V superimposed on a schematic of the hyperboloidal tips. The solid line black represents the exact maximum potential along the emitter surface, the dashed red line represents the average maximum potential ($\psi_{m,av}$), and the dashed blue line represents the corresponding maximum potential for a flat emitter surface ($\psi_{m,flat}$). Here $W = 0.5 \mu\text{m}$, $D = 0.5 \mu\text{m}$, $h = 0.4 \mu\text{m}$, and $R = 0.25 \mu\text{m}$. Plane-averaged (b) current density (J_{tot}) and (c) output power density (P) across the entirety of the square area with respect to the applied voltage (V). Here $D = 0.5 \mu\text{m}$ and $W = 0.5 \mu\text{m}$, and a variety of tip heights and base radii are compared.

D. Energy analysis with constant electrode temperatures

To calculate the TEC's efficiency, we must determine the various energy terms that exchange between the electrodes by establishing an energy balance. Here, we ignore heat loss through the leads and to the ambient environment in order to focus merely on the effect of microstructures on the charge and energy transport between electrodes. The energy terms considered include the energy carried away from the emitter by electrons, Q_E , the energy carried into the collector by electrons, Q_C , and the energy transferred via thermal radiation, Q_R , as shown in Fig. 1(a). Q_E and Q_C are described by the following expressions [1]:

$$Q_E(s) = J_{EC} \frac{\psi_m + 2k_B T_E}{e} - J_{CE} \frac{\psi_m + 2k_B T_C}{e}, \quad (11a)$$

$$Q_C(s) = J_{EC} \frac{\psi_m - eV + 2k_B T_E}{e} - J_{CE} \frac{\psi_m - eV + 2k_B T_C}{e}, \quad (11b)$$

where both terms depend on s due to their dependencies on ψ_m and J . Therefore, the plane-averaged thermionic energy fluxes carried out from the emitter ($i = E$) or carried to the collector ($i = C$) for the tip can be obtained from

$$Q_{i,tip} = \frac{2}{R^2} \int_1^{s_0} Q_i(s) h_s(s) h_\alpha(s) ds. \quad (12)$$

The average energy densities across the square area are then calculated from

$$Q_{i,tot} = \frac{1}{W^2} [\pi R^2 Q_{i,tip} + (W^2 - \pi R^2) Q_{i,flat}], \quad (13)$$

where $Q_{i,flat}$ represents the thermionic energy flux corresponding to the flat area and is appropriately found using the flat area's maximum potential, $\psi_{m,flat}$, and current densities, $J_{EC,flat}$ and $J_{CE,flat}$, in Eq. (11).

Finding Q_R requires the consideration of the evanescent waves' contribution to the radiative heat flux when the gap distance is comparable to the characteristic thermal wavelength of radiation. The net radiative heat flux from the emitter to the collector can be obtained from [15,16]

$$Q_R = \int_{\omega=0}^{\infty} \frac{d\omega}{4\pi^2} [\Theta(\omega, T_E) - \Theta(\omega, T_C)] \times \int_{k_\rho=0}^{\infty} T(\omega, k_\rho) k_\rho dk_\rho \quad (14)$$

where $\Theta(\omega, T) \equiv h\omega / [\exp(h\omega/k_B T) - 1]$ is the mean energy of a Planck oscillator at angular frequency ω , k_ρ is the parallel wave vector, and $T(\omega, k_\rho)$ represents the transmission probability of the electromagnetic waves for both TE modes and TM modes, which depends on the optical properties of the electrodes [15,16]. To evaluate the effect of microstructures on the radiative heat transfer between the electrodes, we assume the electrodes' optical properties to be those of tungsten. The dielectric function of tungsten, ϵ_W , is found using Palik's tabular data and is assumed to be independent of temperature [39].

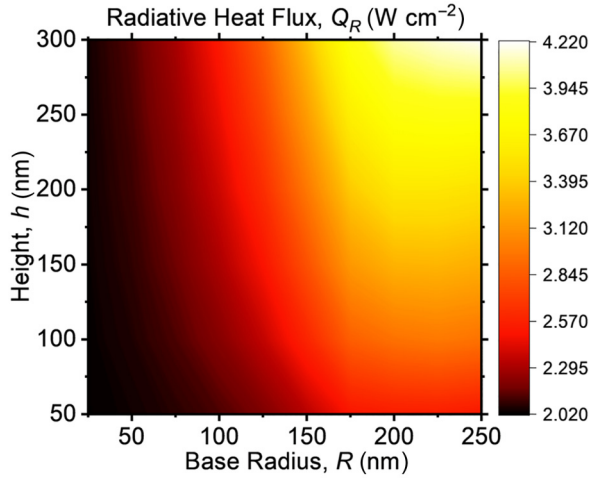


FIG. 4. Relationship of Q_R with the tip height (h) and base radius (R) for a tip periodicity W of $0.5 \mu\text{m}$ and a gap distance D of $0.5 \mu\text{m}$ between the electrodes, which are both assumed to have the optical properties of tungsten.

To account for the change in optical properties brought about by the addition of the hyperboloidal tips, the effective dielectric function, ϵ_{eff} , needs to be calculated with use of the Bruggeman formulation for effective-medium theory [16]:

$$f \frac{\epsilon_W - \epsilon_{\text{eff}}}{\epsilon_W + 2\epsilon_{\text{eff}}} + (1 - f) \frac{\epsilon_{\text{vac}} - \epsilon_{\text{eff}}}{\epsilon_{\text{vac}} + 2\epsilon_{\text{eff}}} = 0, \quad (15)$$

where $\epsilon_{\text{vac}} (= 1)$ is the dielectric constant of a vacuum and f is the filling factor, which can be found from

$$f(x) = \frac{\pi r}{dW^2} [(D - x)^2 - d^2]. \quad (16)$$

After ϵ_{eff} has been found, Q_R can be calculated by following the transfer-matrix method [16,40,41], evaluated at distance d . Figure 4 demonstrates the magnitude of Q_R as a function of h and R , in which the tip heights shown are those where the effective-medium theory is considered valid, i.e., $1 < W/d < \pi$ [42]. Similarly to the output power density, Q_R shows a strong dependence on the surface area, where increasing the base radius has a larger influence on Q_R compared with increasing the height. Since the direction of propagation is normal to the emitter, narrow tips do not increase the heat flux as much as broad tips do for any height. Tall tips with small base radii, despite being closer to the collector, possess ϵ_{eff} closer to ϵ_{vac} than ϵ_W due to their having especially small filling factors throughout.

III. TEC PERFORMANCE

The conversion efficiency, η , is defined as the ratio of the electric power density generated, P , to the total heat

leaving the emitter ($Q_{E,\text{tot}} + Q_R$) [1,4,5]:

$$\eta = \frac{P}{Q_{E,\text{tot}} + Q_R}. \quad (17)$$

Figure 5(a) demonstrates a minimal increase in efficiency gained from the addition of hyperboloidal surface features compared with an emitter with no surface features. The increase in emitting surface area that results in the substantial increase in P also results in an increase in both Q_R (Fig. 4) and $Q_{E,\text{tot}}$. This dual dependency on the tip's surface area is ultimately what limits the increase of efficiency.

To further explore the potential increase of the power output as a function of the geometrical parameters of the features, we calculated the maximum-power points for various values of W and D , as shown in Fig. 5(b). Knowing that P highly depends on S_{tip} , the base radii and tip heights for a given W and D were set to be $R = W/2$ and $h = 0.9D$ for this calculation. Figure 5(b) demonstrates the immense increase gained in maximum output power density when extremely tall and narrow tip geometries are implemented. As the tips get taller and narrower, the increase in emitting surface area follows a nearly identical trend as the maximum-power points. At the point where the greatest increase is seen in Fig. 5(b) ($W = 0.5 \mu\text{m}$, $D = 1 \mu\text{m}$), the maximum output power density is shown to increase by a factor of 3.52, while the surface area at this same point increases by a factor of 3.36 when compared with a planar emitter. The additional increase in maximum power can be explained by the influence of Schottky barrier lowering, which is still minor even for such geometries. It is noteworthy that although Fig. 5(b) implies that power output would continue to increase as D increases and W decreases, this trend is expected to stop at larger separations due to the escalation of negative space charge buildup between the tips and the collector.

While the primary findings of this study have been derived under the assumption of our ignoring NSC effects—based on both literature precedents and the specific scope of our study, particularly considering the complexities and current lack of an analytical solution for accurately including NSC effects in microstructured TECs—it is instructive to provide a brief examination of the simplified estimation of NSC's implications. This serves not only as an additional validation of our method but also offers nuanced insights into the complex interplay between microstructuring and electrostatic effects in thermionic-energy-conversion systems. While the consideration of NSC does introduce a reduction in the absolute power output values, it is critical to note that it does not undermine the primary conclusion of our study—the appreciable increase of power output due to increased surface area with microstructures. Figure 6 elucidates this assertion, illustrating that even in the presence of NSC, the introduction

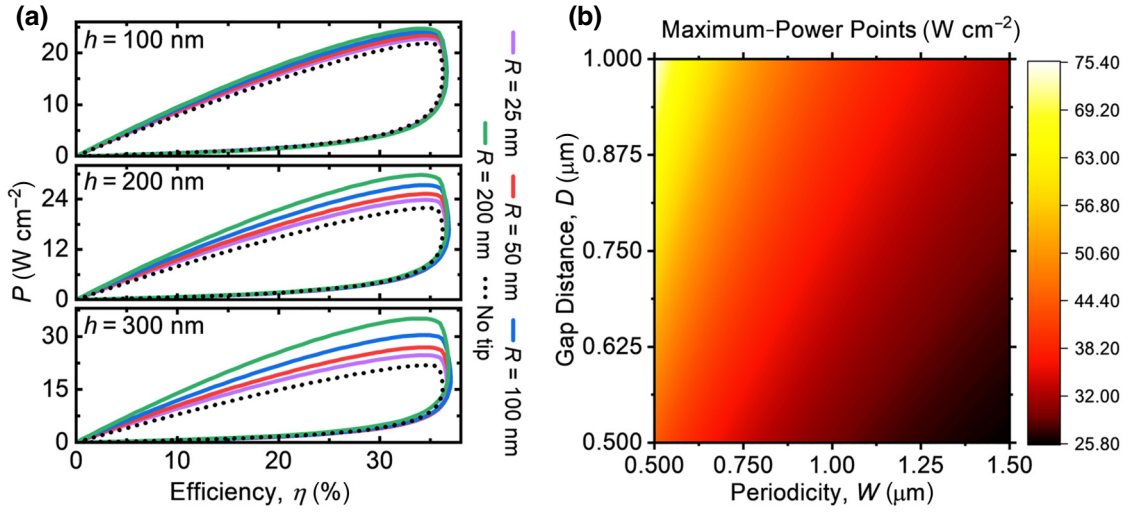


FIG. 5. (a) Output power density (P) versus conversion efficiency (η) for a periodicity W of $0.5 \mu\text{m}$ and a gap distance D of $0.5 \mu\text{m}$ for a variety of different tip heights and base radii. (b) Maximum-power points across a range of periodicities (W) and gap distances (D), where $R = W/2$ and $h = 0.9D$.

of microstructures leads to a considerable increase in output power density. It is important, however, to recognize that this increase is somewhat mitigated by the larger emitting surface area, which contributes to a greater NSC in the interelectrode gap. To substantiate this, consider the case where the dimensions are defined as $D = W = 1.5 \mu\text{m}$ and $R = h/2 = 0.6 \mu\text{m}$. Under these conditions, when NSC is factored in, the maximum-power-density enhancement factor is 1.69 compared with a flat emitter, whereas ignoring NSC yields a slightly higher enhancement factor of 1.77 at the maximum-power point. Notably, as the separation distance D decreases, the disparity between these enhancement factors lessens. This trend aligns with our

hypothesis: at smaller separation distances, the charge buildup between tips becomes less significant, rendering the system's behavior akin to the ideal scenario without NSC.

For the estimations shown in Fig. 6, we adapted a simplified model from our previous study [4], extending it to approximate the NSC effects introduced by the microstructures. This approach, while offering a first-order estimation, is guided by the understanding that a precise analytical solution for NSC in such complex microstructures is currently unavailable. The model focuses on the varying distance from the collector along s , the increased NSC buildup due to the larger emitting surface area, and the geometrical field enhancement. While we use a one-dimensional framework, thus not capturing potential three-dimensional effects, we believe these effects to be minimal in the context of our study. A comprehensive computational analysis, which is beyond the scope of our current model, would be required for a more-accurate depiction of these three-dimensional aspects.

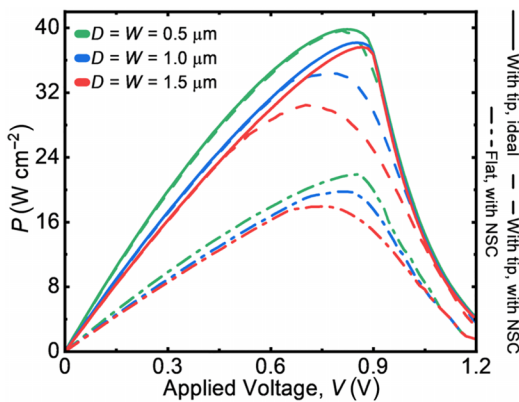


FIG. 6. Comparison of power density as a function of applied voltage (V) in the presence of NSC effects. The data are shown for various periodicities (W) and gap distances (D), with $R = 0.8W/2$ and $h = 0.8D$. This figure elucidates that despite the inclusion of NSC, significant increases in power density are observed with microstructured emitters.

IV. CONCLUSION

In this article, we present a theoretical framework outlining how engineered emitters with microscale surface features can improve the performance of TECs. We considered hyperboloidal tips on the emitter surface of a TEC and studied the charge and thermal radiative transport between the two electrodes separated by a microscale gap distance. By carefully calculating the change in the maximum potential barrier, the effective emitting surface area, and the radiative heat flux, we demonstrated that while the output power density can be significantly increased, the increase in efficiency is limited due to a simultaneous increase in

radiative heat flux. Our results indicate that for most tip geometries, the increase in emitting surface area brought about by the tips has a greater influence than their augmentation of Schottky barrier lowering. We believe this theoretical framework could be applied in future TEC designs to greatly increase their power output.

ACKNOWLEDGMENTS

This work was supported by NSF/EPSCoR RII Track-1: Emergent Quantum Materials and Technologies (EQUATE), Grant No. OIA-2044049. G.A. acknowledges partial support from the NASA Nebraska Space Grant Fellowship and B. A.-A. acknowledges support from the Nebraska Center for Energy Sciences Research and the University of Nebraska–Lincoln Undergraduate Creative Activities and Research Experiences program.

-
- [1] G. N. Hatsopoulos and E. P. Gyftopoulos, *Thermionic Energy Conversion. Volume I: Processes and Devices* (MIT Press, Cambridge, Massachusetts, 1973).
- [2] N. R. Council *et al.*, *Thermionics Quo Vadis?: An Assessment of the DTRA's Advanced Thermionics Research and Development Program* (National Academies Press, Washington, D.C., 2002).
- [3] G. N. Hatsopoulos and E. P. Gyftopoulos, *Thermionic Energy Conversion. Volume II: Processes and Devices* (MIT Press, Cambridge, Massachusetts, 1979).
- [4] M.-E. Dahdolan and M. Ghashami, Comprehensive theoretical framework for the analysis of microgap thermionic energy conversion under constant heat inputs, *Energy Convers. Manage.* **245**, 114600 (2021).
- [5] D. Jensen, A. T. Elahi, M. Ghashami, and K. Park, Submicrometer-gap thermionic power generation based on comprehensive modeling of charge and thermal transport, *Phys. Rev. Appl.* **15**, 024062 (2021).
- [6] J. F. Morris, *Cesium-diode performances from the 1963-to-1971 thermionic conversion specialist conferences*, Tech. Rep. (1972).
- [7] R. Wanke, W. Voesch, I. Rastegar, A. Kyriazis, W. Braun, and J. Mannhart, Thermoelectronic energy conversion: Concepts and materials, *MRS Bulletin* **42**, 518 (2017).
- [8] G. Hassink, R. Wanke, I. Rastegar, W. Braun, C. Stephanos, P. Herlinger, J. Smet, and J. Mannhart, Transparency of graphene for low-energy electrons measured in a vacuum-triode setup, *APL Mater.* **3**, 076106 (2015).
- [9] A. Ziabari, M. Zebarjadi, D. Vashaee, and A. Shakouri, Nanoscale solid-state cooling: A review, *Rep. Prog. Phys.* **79**, 095901 (2016).
- [10] M. F. Campbell, T. J. Celenza, F. Schmitt, J. W. Schwede, and I. Bargatin, Progress toward high power output in thermionic energy converters, *Adv. Sci.* **8**, 2003812 (2021).
- [11] K. L. Jensen, *Introduction to the Physics of Electron Emission* (John Wiley & Sons, Hoboken, New Jersey, 2017).
- [12] J.-H. Lee, I. Bargatin, N. A. Melosh, and R. T. Howe, Optimal emitter-collector gap for thermionic energy converters, *Appl. Phys. Lett.* **100**, 173904 (2012).
- [13] T. Liang, J. Chen, X. Chen, S. Su, and J. Chen, Trade-off between the near-field heat transfer and the space charge effect in graphene-anode thermionic energy converters, *Energy* **260**, 125174 (2022).
- [14] A. H. Khoshaman and A. Nojeh, A self-consistent approach to the analysis of thermionic devices, *J. Appl. Phys.* **119**, 044902 (2016).
- [15] M. Francoeur and M. P. Mengüç, Role of fluctuational electrodynamics in near-field radiative heat transfer, *J. Quant. Spectrosc. Radiat. Transfer* **109**, 280 (2008).
- [16] Z. M. Zhang, Z. M. Zhang, and Luby, *Nano/microscale Heat Transfer* (Springer, New York, New York, 2007), Vol. 410.
- [17] E. Rahman and A. Nojeh, Interplay between near-field radiative coupling and space-charge effects in a microgap thermionic energy converter under fixed heat input, *Phys. Rev. Appl.* **14**, 024082 (2020).
- [18] R. Y. Belbachir, Z. An, and T. Ono, Thermal investigation of a micro-gap thermionic power generator, *J. Micromech. Microeng.* **24**, 085009 (2014).
- [19] A. Bellucci, G. Sabbatella, M. Girolami, M. Mastellone, V. Serpente, A. Mezzi, S. Kaciulis, B. Paci, A. Generosi, R. Polini, A. Vitulano, I. Vivaldi, M. Antonelli, and D. M. Trucchi, Dielectric micro- and sub-micrometric spacers for high-temperature energy converters, *Energy Technol.* **9**, 2000788 (2021).
- [20] M. F. Campbell, M. Azadi, Z. Lu, A. G. Eskenazi, A. Jain, J. W. Bang, P. G. Sieg, G. A. Popov, S. M. Nicaise, K. C. Van Houten, F. Schmitt, J. W. Schwede, and I. Bargatin, Nanostructured spacers for thermionic and thermophotovoltaic energy converters, *J. Microelectromech. Syst.* **29**, 637 (2020).
- [21] K. A. Littau, K. Sahasrabudde, D. Barfield, H. Yuan, Z.-X. Shen, R. T. Howe, and N. A. Melosh, Microbead-separated thermionic energy converter with enhanced emission current, *Phys. Chem. Chem. Phys.* **15**, 14442 (2013).
- [22] J.-H. Lee, I. Bargatin, B. K. Vancil, T. O. Gwinn, R. Maboudian, N. A. Melosh, and R. T. Howe, Microfabricated thermally isolated low work-function emitter, *J. Microelectromech. Syst.* **23**, 1182 (2014).
- [23] M. O. Hassan, K. Takahata, and A. Nojeh, Space charge in a vacuum diode: From macroscopic to microscopic gaps, *J. Appl. Phys.* **130**, 024502 (2021).
- [24] G. O. Fitzpatrick, J. K. Koester, J. Chang, E. J. Britt, and J. B. McVey, in *IECEC 96. Proceedings of the 31st Inter-society Energy Conversion Engineering Conference*, Vol. 2 (IEEE, Washington, D.C., 1996), p. 920.
- [25] H. Yuan, D. C. Riley, Z.-X. Shen, P. A. Pianetta, N. A. Melosh, and R. T. Howe, Back-gated graphene anode for more efficient thermionic energy converters, *Nano Energy* **32**, 67 (2017).
- [26] I. T. Lim, S. A. Lambert, J.-L. Vay, and J. W. Schwede, Electron reflection in thermionic energy converters, *Appl. Phys. Lett.* **112**, 073906 (2018).
- [27] A. L. F. Cauduro, L. H. Hess, D. F. Ogletree, J. W. Schwede, and A. K. Schmid, Tailoring low energy electron absorption via surface nano-engineering of cesiated chromium films, *Appl. Phys. Lett.* **115**, 071602 (2019).
- [28] D. Biswas, G. Singh, S. G. Sarkar, and R. Kumar, Variation of field enhancement factor near the emitter tip, *Ultramicroscopy* **185**, 1 (2018).

- [29] D. Biswas, G. Singh, and R. Kumar, Modeling field emitter arrays using nonlinear line charge distribution, *J. Appl. Phys.* **120**, 124307 (2016).
- [30] D. Biswas, A universal formula for the field enhancement factor, *Phys. Plasmas* **25**, 043113 (2018).
- [31] R. G. Forbes, C. Edgcombe, and U. Valdre, Some comments on models for field enhancement, *Ultramicroscopy* **95**, 57 (2003).
- [32] L.-H. Pan, T. E. Sullivan, V. J. Peridier, P. H. Cutler, and N. M. Miskovsky, Three-dimensional electrostatic potential, and potential-energy barrier, near a tip-base junction, *Appl. Phys. Lett.* **65**, 2151 (1994).
- [33] J. Zuber, K. L. Jensen, and T. Sullivan, An analytical solution for microtip field emission current and effective emission area, *J. Appl. Phys.* **91**, 9379 (2002).
- [34] J. P. Edelen, N. M. Cook, C. C. Hall, Y. Hu, X. Tan, and J.-L. Vay, Advanced modeling of field enhanced thermionic emission, *J. Vac. Sci. Technol. B, Nanotechnology and Microelectronics: Materials, Processing, Measurement, and Phenomena* **38**, 043201 (2020).
- [35] J. Smith, R. Nemanich, and G. Bilbro, The effect of schottky barrier lowering and nonplanar emitter geometry on the performance of a thermionic energy converter, *Diam. Relat. Mater.* **15**, 870 (2006).
- [36] E. Barmina, A. Serkov, E. Stratakis, C. Fotakis, V. Stolyarov, I. Stolyarov, and G. Shafeev, Nano-textured W shows improvement of thermionic emission properties, *Appl. Phys. A* **106**, 1 (2012).
- [37] T. J. Leong, K. A. A. Khalid, and K. Mohamed, A study of SiC nanostructures grown on Si substrate as thermionic cathode and its work function lowering effect, *IEEE Electron Device Lett.* **41**, 1098 (2020).
- [38] G. B. Arfken, *Mathematical Methods for Physicists* (Academic Press, Burlington, Massachusetts, 1970), 2nd ed.
- [39] E. D. Palik, *Handbook of Optical Constants of Solids* (Academic Press, New York, New York, 1998), Vol. 3.
- [40] D. Xu, A. Bilal, J. Zhao, L. Liu, and Z. Zhang, Near-field radiative heat transfer between rough surfaces modeled using effective media with gradient distribution of dielectric function, *Int. J. Heat Mass Transf.* **142**, 118432 (2019).
- [41] S. Li, D. Xu, J. Zhao, and L. Liu, Random rough surface effects on the performance of near-field thermophotovoltaic system, *Int. J. Heat Mass Transf.* **202**, 123713 (2023).
- [42] S. Zare, R. Pouria, and S. Edalatpour, Validity of the effective medium theory for modeling near-field thermal emission by nanowire arrays, *J. Quant. Spectrosc. Radiat. Transfer* **261**, 107482 (2021).